Journal of Computational Physics **180,** 54–77 (2002)
doi:10.1006/jcph.2002.7062

Computation of Multiphase Mixture Flows with Compressibility Effects

Sankaran Venkateswaran,* Jules W. Lindau,† Robert F. Kunz,† and Charles L. Merkle*

*University of Tennessee, Tullahoma, Tennessee 37388; and †The Pennsylvania State University Applied Research Lab, State College, Pennsylvania 16804
E-mail: venkatas@nas.nasa.gov, jwl@wt.arl.psu.edu, rfk@wt.arl.psu.edu, cmerkle@utsi.edu

Received November 6, 2001; revised March 25, 2002

A time-marching computational fluid dynamics method is developed and applied to the computation of multiphase mixture flows. The model accounts for finite acoustic speeds in the constituent phases, which typically lead to transonic/supersonic flow and associated compressibility phenomena such as shock formation in the mixture region. Preconditioning or artificial compressibility methods are devised using perturbation theory to insure that the method retains efficiency and accuracy in both the incompressible and compressible flow regimes. The resulting algorithm is incorporated within an existing multiphase code, and several representative applications are used to demonstrate the capabilities of the method. In particular, our results suggest that the present compressible formulation provides an improved description of cavitation dynamics compared with previous incompressible computations.

Key Words: preconditioning, artificial compressibility methods; multiphase, homogeneous mixture models; compressibility effects.

1. INTRODUCTION

Multiphase flows are encountered in a wide range of applications involving heat exchange, cavitation, sprays, porous media, etc. The computation of multiphase flows has received growing research attention in recent years, due in part to the evolving maturity of single-phase computational fluid dynamics (CFD) algorithms. There remain, however, several physical and modeling challenges. A primary issue is the strong coupling of acoustic phenomena [1–5] due to the fact that the speed of sound in two-phase mixtures can be extremely low compared to the sound speeds in the individual component phases. Thus, multiphase flows are frequently characterized by local regions, wherein the flow may be transonic or even supersonic with the presence of shocks, although the bulk of the flow may remain essentially incompressible. This situation presents a unique challenge to the

0021-9991/02 $35.00

design of CFD algorithms. The development of appropriate numerical schemes for such multiphase problems is the subject of the present paper.

There are many levels of modeling that may be used in multiphase computations [6]. In general, one may distinguish between methods that employ an Eulerian framework for all phases and those that employ Eulerian for a carrier phase and Lagrangian for disperse phases. In the liquid–vapor, Eulerian–Eulerian framework, the simplest approach is to employ a single continuity equation for both phases, with the fluid density being described as a continuous function varying between the vapor and liquid phases [7–9]. At a more detailed level of modeling, separate continuity equations for the liquid and vapor phases are employed along with appropriate mass transfer terms to represent the phase-change phenomena [10–14]. The gas–liquid interface is, however, assumed to be in dynamic and thermal equilibrium and, consequently, mixture momentum and energy equations are used. This model is usually referred to as the homogeneous mixture model [6] and is the level of modeling considered in this paper. The model is appropriate for developed, attached cavitation in hydrodynamics applications, the area of primary interest to us, due to the relatively large cavity sizes and negligible surface tension effects in these flows. Finally, we note that full multifluid modeling, involving separate momentum and energy equations for each of the phases, has also been used for certain classes of multiphase flow [6] but is not addressed here.

The crucial requirement of multiphase algorithms is the ability to accurately and efficiently span both incompressible and compressible flow regimes. For single-phase applications, time-marching techniques have long been established as the methods of choice for high-speed compressible flows, while artificial compressibility or, more generally, preconditioning techniques have enabled the extension of these methods to the incompressible and low-speed compressible regimes [15–18]. Preconditioning methods introduce appropriate pseudo-time-derivatives in order to maintain proper conditioning of the controlling acoustic and particle convection timescales. Indeed, it is now widely recognized that the careful selection of these derivatives is crucial for ensuring both efficiency and accuracy over a wide range of Mach numbers, Reynolds numbers, and Strouhal numbers [18]. Here, we are concerned with the extension of preconditioned time-marching approaches to the multiphase system.

Several researchers have previously reported algorithms for multiphase mixtures. Merkle *et al.* developed a preconditioning formulation, using mass fraction as the dependent variable [10]. Kunz *et al.* developed an alternate preconditioning formulation, using volume fraction as the dependent variable [11]. In these formulations, constant densities were assumed for each of the liquid and vapor phases, and compressibility effects were not accounted for in the two-phase mixture region. Ahuja *et al.* have developed a multiphase preconditioning algorithm, including compressibility effects in the component phases [13]. Likewise, Senocak and Shyy have developed a pressure-based algorithm accounting for compressibility effects [14]. Both these latter models are concerned with the so-called *isothermal compressible* situation, wherein the densities of the fluids are assumed to be functions of the pressure, but not the temperature, and therefore the energy equation is not solved. In the present paper, the isothermal compressible multiphase system is the level of modeling adopted. The specific focus here is the understanding of the time-marching system characteristics and the derivation of appropriately scaled preconditioning forms to facilitate numerical computations.

Perturbation theory is an invaluable analytical tool for probing the behavior of the fluid dynamics equations under limiting flow conditions [18]. Importantly, it provides a means

of formally deriving appropriately scaled preconditioning forms for insuring convergence efficiency, thereby eliminating the guesswork from the process. Moreover, the perturbation analysis may also be extended to the *discrete* version of the system to elucidate the importance of properly scaled equations for insuring accuracy under limiting flow conditions [18]. In this paper, we employ perturbation theory to analyze the multiphase system. We show that the preconditioning methodology is not unique, and depending upon the precise form of the governing equations used in the derivation, we obtain related but distinct preconditioning formulations. In fact, these formulations are generalizations of the preconditioning forms mentioned earlier and include the isothermal compressible system of Ahuja *et al.* [13] as well as the isothermal compressible extensions of the Merkle *et al.* [10] and Kunz *et al.* [11] systems. Indeed, our analysis shows that all of these approaches promise similar convergence properties and properly preserve the accuracy of the discrete formulation.

The paper is organized as follows. We begin with the equations of motion for two-phase homogeneous mixture flows. The equations are presented both in their volume fraction and mass fraction forms. We examine the eigenvalues of these systems to assess the conditioning of the system in the compressible and incompressible limits. We then employ perturbation theory to probe the underlying sources of stiffness and devise preconditioning forms that maintain well-conditioned behavior in both compressible and incompressible flow regimes. Our primary interest lies in sheet- and super-cavitating flows encountered in naval hydrodynamics applications. These flows are typically turbulent and also exhibit large-scale unsteadiness. Accordingly, the multiphase algorithm derived in this paper is incorporated into a dual-time framework for time accuracy [16]. In Results, the method is then applied to various applications of interest, including cavitating flows over axisymmetric ogive configurations for which measurement data are available. Finally, we conclude with a summary and a brief description of current and future work.

2. EQUATIONS OF MOTION

2.1. Volume Fraction Form

The governing equations for two-phase flow are customarily written in terms of volume fraction variables. For the purposes of the theoretical derivation, we employ only the one-dimensional inviscid flow equations, although in practical implementation, the multidimensional Reynolds-averaged equations are used. We also drop the source terms describing the mass transfer between the phases and again the relevant terms will be introduced in practical implementation. The individual continuity equations for the vapor and liquid phases are

$$\frac{\partial \tilde{\rho}_v \alpha_v}{\partial \tau} + \frac{\partial \tilde{\rho}_v \alpha_v u}{\partial x} = 0 \tag{1}$$

$$\frac{\partial \tilde{\rho}_l \alpha_l}{\partial \tau} + \frac{\partial \tilde{\rho}_l \alpha_l u}{\partial x} = 0, \tag{2}$$

while the global momentum equation is

$$\frac{\partial \rho u}{\partial \tau} + \frac{\partial \rho u^2}{\partial x} + \frac{\partial p}{\partial x} = 0. \tag{3}$$

In the above equations, the mixture density is defined as

$$\rho = \tilde{\rho}_l \alpha_l + \tilde{\rho}_v \alpha_v, \tag{4}$$

while the individual phasic densities, $\tilde{\rho}_v$ and $\tilde{\rho}_l$, are defined as mass of the phase per unit volume occupied by that phase. Also, we note that $\alpha_v + \alpha_l = 1$. The system is then closed by the phasic equations of state,

$$\tilde{\rho}_v = \tilde{\rho}_v(p) \qquad \text{and} \qquad \tilde{\rho}_l = \tilde{\rho}_l(p), \tag{5}$$

where the individual phasic densities are assumed to be functions of pressure only. In our previous work [11, 12], these quantities were taken to be constant, representing a mixture of incompressible phases.

2.2. Mass Fraction Form

The above equations may alternatively be written in terms of mass fraction variables as well. This form is customarily used for gaseous mixtures but is also equally valid for general multiphase mixtures.

$$\frac{\partial \rho Y_v}{\partial \tau} + \frac{\partial \rho Y_v u}{\partial x} = 0 \tag{6}$$

$$\frac{\partial \rho Y_l}{\partial \tau} + \frac{\partial \rho Y_l u}{\partial x} = 0, \tag{7}$$

with the momentum equation having the same form as Eq. (3).

It is sometimes useful to define the individual phasic densities, $\rho_v = \rho Y_v$ and $\rho_l = \rho Y_l$, which are given as the mass of phase per unit volume occupied by the mixture. Note that these phasic densities are distinct from those introduced earlier and are related by the following expressions:

$$\rho_v = \tilde{\rho}_v \alpha_v \qquad \rho_l = \tilde{\rho}_l \alpha_l. \tag{8}$$

Further, the mixture density, $\rho = \rho_v + \rho_l$, and $Y_v + Y_l = 1$. It is straightforward to see that the mass and volume fraction forms are in fact identical.

In the case of gaseous mixtures, it is customary to replace one of the phasic (or species) continuity equations by an overall continuity equation (obtained by summing up the individual continuity equations):

$$\frac{\partial \rho}{\partial \tau} + \frac{\partial \rho u}{\partial x} = 0. \tag{9}$$

However, for multiphase flows, this procedure is prone to error because of difficulties in accurately computing small changes in the vapor density (ρ_v) from differences between the relatively large overall (ρ) and liquid (ρ_l) densities. It is therefore advisable to solve the individual phasic continuity equations directly.

Alternately, some researchers prefer to define an overall mixture volume continuity equation, obtained by dividing the phasic continuity equations by the respective phasic densities

and then summing them up:

$$\frac{1}{\tilde{\rho}_v}\frac{\partial \tilde{\rho}_v \alpha_v}{\partial \tau} + \frac{1}{\tilde{\rho}_l}\frac{\partial \tilde{\rho}_l \alpha_l}{\partial \tau} + \frac{1}{\tilde{\rho}_v}\frac{\partial \tilde{\rho}_v \alpha_v u}{\partial x} + \frac{1}{\tilde{\rho}_l}\frac{\partial \tilde{\rho}_l \alpha_l u}{\partial x} = 0. \tag{10}$$

For purposes of solution, in this paper, we employ the volume fraction system with all the individual phasic continuity equations. However, the mass fraction and the overall mixture continuity forms are useful for purposes of analysis, as evident in the following sections.

3. EIGENVALUE ANALYSIS

3.1. Volume Fraction Form

The system given in Eqs. (1)–(3) may be expressed in the vector form

$$\Gamma_\alpha \frac{\partial Q_\alpha}{\partial \tau} + \frac{\partial E}{\partial x} = 0, \tag{11}$$

where

$$Q_\alpha = \begin{bmatrix} p \\ \alpha_v \\ u \end{bmatrix} \qquad E = \begin{bmatrix} \tilde{\rho}_v \alpha_v u \\ \tilde{\rho}_l \alpha_l u \\ \rho u^2 + p \end{bmatrix} \qquad \Gamma_\alpha = \begin{bmatrix} \alpha_v \frac{\partial \tilde{\rho}_v}{\partial p}\Big|_{\alpha_v} & \tilde{\rho}_v & 0 \\ \alpha_l \frac{\partial \tilde{\rho}_l}{\partial p}\Big|_{\alpha_v} & -\tilde{\rho}_l & 0 \\ u \frac{\partial \rho}{\partial p}\Big|_{\alpha_v} & u(\tilde{\rho}_v - \tilde{\rho}_l) & \rho \end{bmatrix}. \tag{12}$$

Note that, for the isothermal system under consideration here, the functions $\partial \tilde{\rho}_v / \partial \rho$ and $\partial \tilde{\rho}_l / \partial \rho$ represent the reciprocal of the squares of the speed of sound in the two individual phases. Also note that

$$\left.\frac{\partial \rho}{\partial p}\right|_{\alpha_v} = \alpha_v \left.\frac{\partial \tilde{\rho}_v}{\partial p}\right|_{\alpha_v} + \alpha_l \left.\frac{\partial \tilde{\rho}_l}{\partial p}\right|_{\alpha_v}. \tag{13}$$

To determine the eigenvalues of the above two-phase system, we define the Jacobian

$$A_\alpha = \frac{\partial E}{\partial Q_\alpha} = \begin{bmatrix} u\alpha_v \frac{\partial \tilde{\rho}_v}{\partial p}\Big|_{\alpha_v} & u\tilde{\rho}_v & \tilde{\rho}_v \alpha_v \\ u\alpha_l \frac{\partial \tilde{\rho}_l}{\partial p}\Big|_{\alpha_v} & -u\tilde{\rho}_l & \tilde{\rho}_l \alpha_l \\ 1 + u^2 \frac{\partial \rho}{\partial p}\Big|_{\alpha_v} & u^2(\tilde{\rho}_v - \tilde{\rho}_l) & \rho u \end{bmatrix}. \tag{14}$$

The system eigenvalues are then given by the eigenvalues of $\Gamma_\alpha^{-1}(A_\alpha)$,

$$\Gamma_\alpha^{-1} A_\alpha = \begin{bmatrix} u & 0 & \rho c^2 \\ 0 & u & Z \\ \frac{1}{\rho} & 0 & u \end{bmatrix} \tag{15}$$

where

$$Z = \rho c^2 \alpha_l \alpha_v \left(\frac{1}{\tilde{\rho}_l}\left.\frac{\partial \tilde{\rho}_l}{\partial p}\right|_{\alpha_v} - \frac{1}{\tilde{\rho}_v}\left.\frac{\partial \tilde{\rho}_v}{\partial p}\right|_{\alpha_v} \right), \tag{16}$$

and the sound speed is given by the expression

$$\frac{1}{c^2} = \rho\left(\frac{\alpha_l}{\tilde{\rho}_l}\frac{\partial\tilde{\rho}_l}{\partial p}\bigg|_{\alpha_v} + \frac{\alpha_v}{\tilde{\rho}_v}\frac{\partial\tilde{\rho}_v}{\partial p}\bigg|_{\alpha_v}\right), \tag{17}$$

which is the standard mixture rule for the sound speed of two-phase mixtures.

It can be readily seen that the eigenvalues of the above system are given as

$$\lambda\left(\Gamma_\alpha^{-1}A_\alpha\right) = u, \qquad u \pm c, \tag{18}$$

which has the familiar form of the single-phase compressible system.

3.2. Mass Fraction Form

The mass-fraction equation system may be expressed in the vector form

$$\Gamma_Y\frac{\partial Q_Y}{\partial\tau} + \frac{\partial E}{\partial x} = 0, \tag{19}$$

where

$$Q_Y = \begin{bmatrix} p \\ Y_v \\ u \end{bmatrix} \qquad E = \begin{bmatrix} \rho Y_v u \\ \rho Y_l u \\ \rho u^2 + p \end{bmatrix} \qquad \Gamma_Y = \begin{bmatrix} Y_v\frac{\partial\rho}{\partial p}\big|_{Y_v} & \rho + Y_v\frac{\partial\rho}{\partial Y_v}\big|_p & 0 \\ Y_l\frac{\partial\rho}{\partial p}\big|_{Y_v} & -\rho + Y_l\frac{\partial\rho}{\partial Y_v}\big|_p & 0 \\ u\frac{\partial\rho}{\partial p}\big|_{Y_v} & u\frac{\partial\rho}{\partial Y_v}\big|_p & \rho \end{bmatrix}. \tag{20}$$

The Jacobian A_Y is given by

$$A_Y = \frac{\partial E}{\partial Q_Y} = \begin{bmatrix} uY_v\frac{\partial\rho}{\partial p}\big|_{Y_v} & \rho u + uY_v\frac{\partial\rho}{\partial Y_v}\big|_p & \rho Y_v \\ uY_l\frac{\partial\rho}{\partial p}\big|_{Y_v} & -\rho u + uY_l\frac{\partial\rho}{\partial Y_v}\big|_p & \rho Y_l \\ 1 + u^2\frac{\partial\rho}{\partial p}\big|_{Y_v} & u^2\frac{\partial\rho}{\partial Y_v}\big|_p & \rho u \end{bmatrix}. \tag{21}$$

The system eigenvalues are then given by the eigenvalues of $\Gamma_Y^{-1}(A_Y)$,

$$\Gamma_Y^{-1}A_y = \begin{bmatrix} u & 0 & \rho c^2 \\ 0 & u & 0 \\ \frac{1}{\rho} & 0 & u \end{bmatrix}, \tag{22}$$

and the sound speed is defined by the expression

$$\frac{1}{c^2} = \frac{\partial\rho}{\partial p}\bigg|_{Y_v}. \tag{23}$$

It is evident that the eigenvalues of the above matrix system are

$$\lambda\left(\Gamma_Y^{-1}A_Y\right) = u, \qquad u \pm c, \tag{24}$$

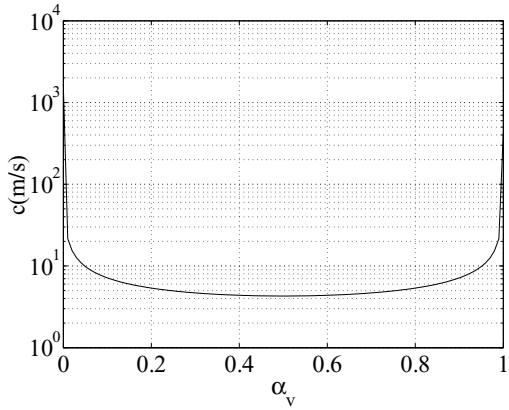

FIG. 1. Mixture sound speed versus vapor volume fraction for equilibrium saturated steam at 300 K.

which are, of course, the same as those given in Eq. (18) because the matrices are similar. Further, it can be easily shown that the property Jacobians are given as

$$\left.\frac{\partial \rho}{\partial p}\right|_{Y_v} = \rho\left(\frac{\alpha_l}{\tilde{\rho}_l}\left.\frac{\partial \tilde{\rho}_l}{\partial p}\right|_{\alpha_v} + \frac{\alpha_v}{\tilde{\rho}_v}\left.\frac{\partial \tilde{\rho}_v}{\partial p}\right|_{\alpha_v}\right) \tag{25}$$

$$\left.\frac{\partial \rho}{\partial Y_v}\right|_{p} = \rho^2\left(\frac{1}{\tilde{\rho}_l} - \frac{1}{\tilde{\rho}_v}\right), \tag{26}$$

where the properties have been expressed in terms of known properties of the two phases. Note that the expression for the speed of sound can be verified to be identical to that in Eq. (17).

From Eq. (17) or (25), it is clear that the speed of sound is significantly attenuated in two-phase mixture regions as shown in Fig. 1. Multiphase flowfields are therefore characterized by widely different flow regimes, i.e., incompressible in the pure liquid phase, low-Mach compressible in the pure vapor phase, and transonic or supersonic in the mixture region. Consequently, it is necessary for the underlying numerical algorithm to be able to handle such widely diverse flow regimes. We point out here that our analysis has been restricted to the inviscid physics of the multiphase system. Viscous and source term effects can indeed influence the nature of the physics (and the numerics) of model, multiphase flowfields, but in many instances, these effects are secondary. In the interests of simplicity, we therefore neglect these effects in our analysis. In the following section, we apply perturbation analysis to probe the underlying character of the time-dependent multiphase system and to derive appropriate preconditioning forms.

4. PERTURBATION ANALYSIS

The perturbation procedure closely follows that developed for the single-phase equations [18]. We consider only the inviscid equations here, although similar developments are possible for the Navier–Stokes equations as well. We begin with the momentum equation, which has a common form in all of the systems described in the above sections. Following that, we consider the various forms of the phasic continuity equations.

4.1. Overall Momentum Equation

We write the equation in the nonconservative form for simplicity:

$$\rho \frac{\partial u}{\partial \tau} + \rho u \frac{\partial u}{\partial x} + \frac{\partial p}{\partial x} = 0. \tag{27}$$

We next nondimensionalize the equations to facilitate order-of-magnitude comparisons between the terms. We introduce the following reference scales for the variables:

$$L, u_r, \tau_r, p_r, \rho_r, \rho_{vr}, \rho_{lr}.$$

Here, L represents a characteristic length scale, u_r is the reference velocity, and τ_r is the reference timescale (defined below). p_r is the reference pressure, while ρ_r is the reference mixture density. Further, we note that ρ_{vr} and ρ_{lr} are the reference phasic densities. The nondimensionalized version of Eq. (27) is then given by

$$\left(\frac{L}{u_r \tau_r}\right) \bar{\rho} \frac{\partial \bar{u}}{\partial \bar{\tau}} + \bar{\rho} \bar{u} \frac{\partial \bar{u}}{\partial \bar{x}} + \left(\frac{p_r}{\rho_r u_r^2}\right) \frac{\partial \bar{p}}{\partial \bar{x}} = 0, \tag{28}$$

where the overbars indicate nondimensional quantities.

We note that the coefficient of the pressure gradient term in the above equation becomes very large in the limit of low-speed flows. To insure that the pressure gradient is always balanced by the convective terms, we define the small parameter

$$\varepsilon = \frac{\rho_r u_r^2}{p_r} \tag{29}$$

and consider the limiting form of Eq. (28) as this parameter goes to zero. We then expand the pressure in a power series,

$$\bar{p} = \bar{p}_0 + \varepsilon \bar{p}_1 + \cdots, \tag{30}$$

and substitute it into Eq. (28) to get

$$\left(\frac{L}{u_r \tau_r}\right) \bar{\rho} \frac{\partial \bar{u}}{\partial \bar{\tau}} + \bar{\rho} \bar{u} \frac{\partial \bar{u}}{\partial \bar{x}} + \frac{1}{\varepsilon} \frac{\partial (\bar{p}_0 + \varepsilon \bar{p}_1)}{\partial \bar{x}} = 0. \tag{31}$$

A more complete procedure would use analogous expansions for all the variables, but the results show that only the zeroth order quantities of the remaining variables appear in the final equations. Consequently, to minimize the algebra, we perturb only the pressure.

The purpose of the time-derivatives in a time-marching scheme is to drive the equations to the desired steady state solution. To insure that this process is efficient, we select the characteristic timescale such that the time-derivatives are of the same magnitude as the convective terms. Specifically, in Eq. (31), the coefficient of the time-derivative must be of order unity so that $\tau_r = L/u_r$. This requirement clearly implies that the appropriate timescale is the convective timescale of the fluid particle. In that case, there remains no term to balance the $1/\varepsilon$ term in the pressure gradient term, leading us to conclude that

$$\frac{\partial \bar{p}_0}{\partial \bar{x}} = 0. \tag{32}$$

Moreover, for most problems, $\bar{p}_0$ is fixed by the boundary condition, and hence this quantity is independent of time as well.

The zeroth order momentum equation therefore takes the form

$$\bar{\rho}\frac{\partial \bar{u}}{\partial \bar{\tau}} + \bar{\rho}\bar{u}\frac{\partial \bar{u}}{\partial \bar{x}} + \frac{\partial \bar{p}_1}{\partial \bar{x}} = 0. \tag{33}$$

Note that the ε term in the pressure gradient has been cancelled by the $1/\varepsilon$ term that multiples it. All the terms in Eq. (33) are clearly of order unity. In the time-marching framework, it is evident that this equation provides an adequate means of updating the velocity $\bar{u}$. However, the presence of the first-order pressure $\bar{p}_1$ implies that we must have a viable way of updating it from the phasic continuity equations. Accordingly, we consider these equations next.

4.2. Phasic Continuity Equations in Volume Fraction Form

To analyze the scaling of the continuity equations, we first consider the volume fraction form given in Eq. (11). After nondimensionalization and perturbation expansions, these equations take the form

$$\left(\frac{p_r}{\rho_{vr}}\frac{\partial \tilde{\rho}_v}{\partial p}\bigg|_{\alpha_v}\right)\alpha_v\varepsilon\frac{\partial \bar{p}_1}{\partial \bar{\tau}} + \bar{\rho}_v\frac{\partial \alpha_v}{\partial \bar{\tau}} + \frac{\partial \bar{\rho}_v\bar{u}\alpha_v}{\partial \bar{x}} = 0 \tag{34}$$

$$\left(\frac{p_r}{\rho_{lr}}\frac{\partial \tilde{\rho}_l}{\partial p}\bigg|_{\alpha_v}\right)\alpha_l\varepsilon\frac{\partial \bar{p}_1}{\partial \bar{\tau}} - \bar{\rho}_l\frac{\partial \alpha_v}{\partial \bar{\tau}} + \frac{\partial \bar{\rho}_l\bar{u}\alpha_l}{\partial \bar{x}} = 0. \tag{35}$$

Note that the phasic volume fractions are already nondimensional terms. Since both equations have time-derivatives of the volume fraction (α_v) that are of order unity, these equations clearly provide a viable manner of updating this variable. The other volume fraction, (α_l), is readily obtained by the relation $\alpha_l = 1 - \alpha_v$. Further, both of the above equations have time-derivatives of the first-order pressure term present. However, these time-derivatives become vanishingly small in the limit of $\varepsilon \to 0$. Thus, in this limit, there is no means of reliably updating the first-order pressure. In practice, the problem manifests itself in slow convergence of the time-marching procedure at low speeds. We further note that the situation is precisely the same as the singularity encountered by the single-phase equations in the incompressible limit.

A further consequence of the singularity in the low-speed limit is a possible degradation in the accuracy of the discrete formulation. This problem has been studied in the context of single-phase flows and shown to be related to the conditioning of the artificial dissipation terms [16, 18]. The traditional way of alleviating the efficiency and accuracy problems is to alter the time-marching system such that it remains well conditioned at all speeds. In the present context, this may be achieved through the introduction of pseudo-property terms in the pressure time-derivative terms such that they are of order unity. Thus,

$$\frac{\partial \bar{\rho}'_v}{\partial p}\bigg|_{\alpha_v} = \frac{\rho_{vr}}{p_r}\frac{1}{\varepsilon} = \frac{\rho_{vr}}{\rho_r}\frac{1}{u_r^2} \tag{36}$$

$$\frac{\partial \bar{\rho}'_l}{\partial p}\bigg|_{\alpha_v} = \frac{\rho_{lr}}{p_r}\frac{1}{\varepsilon} = \frac{\rho_{lr}}{\rho_r}\frac{1}{u_r^2}. \tag{37}$$

The above scaling insures that each of the pressure time-derivatives in Eqs. (34) and (35) are of order unity in the asymptotic limit of $\varepsilon \to 0$. The time-dependent system is thereby rendered suitable for time-marching computations at all flow speeds. This scaling procedure is generally referred to as preconditioning, and in the single-phase case, it precisely corresponds to the artificial compressibility formulation [15–18].

4.3. Overall Mixture Volume Continuity Equation

Other preconditioning scalings result when different forms of the governing equations are used. For instance, if the overall mixture volume continuity equation (given in Eq. (10)) is used, we get the following equation after nondimensionalization and perturbation expansions:

$$\left[\left(\frac{p_r}{\rho_{vr}}\frac{\partial\tilde{\rho}_v}{\partial p}\bigg|_{\alpha_v}\right)\frac{\alpha_v}{\bar{\rho}_v} + \left(\frac{p_r}{\rho_{lr}}\frac{\partial\tilde{\rho}_l}{\partial p}\bigg|_{\alpha_v}\right)\frac{\alpha_l}{\bar{\rho}_l}\right]\varepsilon\frac{\partial\bar{p}_1}{\partial\bar{\tau}} + \frac{1}{\bar{\rho}_v}\frac{\partial\bar{\rho}_v\bar{u}\alpha_v}{\partial\bar{x}} + \frac{1}{\bar{\rho}_l}\frac{\partial\bar{\rho}_l\bar{u}\alpha_l}{\partial\bar{x}} = 0. \quad (38)$$

Note that the above equation serves as a means for updating only the first-order pressure since the volume fraction no longer appears in the time-derivative. Thus, one of the individual phasic continuity equations will serve to update the volume fraction.

For Eq. (38) to be well behaved as $\varepsilon \to 0$, we must require that the term in square brackets be scaled so that it is on the order of $1/\varepsilon$. One way of doing this is to use the scalings suggested in Eqs. (36) and (37). However, a different scaling also becomes possible. Consider

$$\frac{\partial\tilde{\rho}'_v}{\partial p}\bigg|_{\alpha_v} = \frac{1}{M_r^2}\frac{\partial\tilde{\rho}_v}{\partial p}\bigg|_{\alpha_v} \quad (39)$$

$$\frac{\partial\tilde{\rho}'_l}{\partial p}\bigg|_{\alpha_v} = \frac{1}{M_r^2}\frac{\partial\tilde{\rho}_l}{\partial p}\bigg|_{\alpha_v}, \quad (40)$$

where $M_r^2 = u_r^2/c_r^2$. Substituting Eqs. (39) and (40) into Eq. (38), we get

$$\left[\left(\frac{\alpha_v}{\tilde{\rho}_v}\frac{\partial\tilde{\rho}_v}{\partial p}\bigg|_{\alpha_v}\right) + \left(\frac{\alpha_l}{\tilde{\rho}_l}\frac{\partial\tilde{\rho}_l}{\partial p}\bigg|_{\alpha_v}\right)\right]\frac{\varepsilon p_r}{M_r^2}\frac{\partial\bar{p}_1}{\partial\bar{\tau}} + \frac{1}{\bar{\rho}_v}\frac{\partial\bar{\rho}_v\bar{u}\alpha_v}{\partial\bar{x}} + \frac{1}{\bar{\rho}_l}\frac{\partial\bar{\rho}_l\bar{u}\alpha_l}{\partial\bar{x}} = 0. \quad (41)$$

Using Eq. (17) and noting that $\varepsilon p_r/\rho_r c_r^2 M_r^2 = 1$, the above equation reduces to

$$\frac{1}{\bar{\rho}\bar{c}^2}\frac{\partial\bar{p}_1}{\partial\bar{\tau}} + \frac{1}{\bar{\rho}_v}\frac{\partial\bar{\rho}_v\bar{u}\alpha_v}{\partial\bar{x}} + \frac{1}{\bar{\rho}_l}\frac{\partial\bar{\rho}_l\bar{u}\alpha_l}{\partial\bar{x}} = 0. \quad (42)$$

The first-order pressure may thus be reliably obtained from the mixture volume continuity equation.

4.4. Phasic Continuity Equations in Mass Fraction Form

Yet another scaling suggests itself if we use the mass fraction form of the phasic continuity equations. After nondimensionalization and perturbation expansions, these equations

become

$$\left(\frac{p_r}{\rho_r}\frac{\partial\rho}{\partial p}\bigg|_{Y_v}\right)Y_v\varepsilon\frac{\partial\bar{p}_1}{\partial\bar{\tau}}+\left(\bar{\rho}+\frac{Y_v}{\rho_r}\frac{\partial\rho}{\partial Y_v}\bigg|_{p}\right)\frac{\partial Y_v}{\partial\bar{\tau}}+\frac{\partial\bar{\rho}\bar{u}Y_v}{\partial\bar{x}}=0 \tag{43}$$

$$\left(\frac{p_r}{\rho_r}\frac{\partial\rho}{\partial p}\bigg|_{Y_v}\right)Y_l\varepsilon\frac{\partial\bar{p}_1}{\partial\bar{\tau}}+\left(-\bar{\rho}+\frac{Y_l}{\rho_r}\frac{\partial\rho}{\partial Y_v}\bigg|_{p}\right)\frac{\partial Y_v}{\partial\bar{\tau}}+\frac{\partial\bar{\rho}\bar{u}Y_l}{\partial\bar{x}}=0. \tag{44}$$

Again, these equations serve as a means of updating the mass fraction variable and the first-order pressure. The former is readily done, while the pressure update is singular in the limit of $\varepsilon\to 0$. In order to remedy this, we introduce pseudo-properties, as we did before. Here, this is readily accomplished by the following scaling:

$$\frac{\partial\rho'}{\partial p}\bigg|_{Y_v}=\frac{\rho_r}{p_r}\frac{1}{\varepsilon}=\frac{1}{u_r^2}. \tag{45}$$

It may be readily verified that introducing this pseudo-property in lieu of the physical derivative $\partial\rho/\partial p$ renders the pressure time-derivatives to be of order unity and thereby amenable to reliable pressure updates.

In the above analyses, we have applied perturbation theory to the continuous (differential) form of the governing equations and verified the appropriate scaling of time-derivatives for efficient time-marching procedures. In order to verify that such rescaled equations preserve the accuracy of the numerical solutions, it is also possible to extend such analyses to the discrete form of the equations. Reference [18] provides details of the discrete analysis for the single-phase equations, and the procedure is similar for the multiphase system. For reasons of brevity, we do not provide the details of the derivation and simply state that discrete analysis of all the preconditioning systems derived here indeed verifies that these systems properly preserve numerical accuracy under the limiting conditions of interest.

5. PRECONDITIONING FORMULATION

In the previous section, we used perturbation analysis to analyze the asymptotic behavior of the governing equations. In particular, we derived various preconditioning or artificial compressibility formulations that render the system well behaved for time-marching solutions. In this section, we summarize the preconditioning formulations and verify that the eigenvalues of the preconditioned systems are indeed well behaved and well conditioned. We emphasize that, although the present analysis is concerned with obtaining steady solutions, the preconditioning formulation may be readily generalized to time-accurate problems using a dual-time approach. Details of the preconditioned dual-time formulation are given in Ref. [18].

5.1. Volume Fraction Form

The preconditioned version of the volume fraction form given in Eq. (11) is obtained by introducing pseudo-properties into the matrix premultiplying the time-derivatives. Thus, we have

$$\Gamma_\alpha^p\frac{\partial Q_\alpha}{\partial\tau}+\frac{\partial E}{\partial x}=0, \tag{46}$$

with the preconditioning matrix being defined as

$$\Gamma_\alpha^p = \begin{bmatrix} \alpha_v \frac{\partial \tilde{\rho}_v'}{\partial p}\Big|_{\alpha_v} & \tilde{\rho}_v & 0 \\ \alpha_l \frac{\partial \tilde{\rho}_l'}{\partial p}\Big|_{\alpha_v} & -\tilde{\rho}_l & 0 \\ u \frac{\partial \rho'}{\partial p}\Big|_{\alpha_v} & u(\tilde{\rho}_v - \tilde{\rho}_l) & \rho \end{bmatrix}. \tag{47}$$

The pseudo-properties are defined so as to render the eigenvalues well conditioned.

One possible choice suggested by Eqs. (36) and (37) is:

$$\left.\frac{\partial \tilde{\rho}_v'}{\partial p}\right|_{\alpha_v} = \frac{\tilde{\rho}_v}{\rho}\frac{1}{V_p^2}, \qquad \left.\frac{\partial \tilde{\rho}_l'}{\partial p}\right|_{\alpha_v} = \frac{\tilde{\rho}_l}{\rho}\frac{1}{V_p^2} \tag{48}$$

$$\left.\frac{\partial \tilde{\rho}'}{\partial p}\right|_{\alpha_v} = \alpha_v \left.\frac{\partial \tilde{\rho}_v'}{\partial p}\right|_{\alpha_v} + \alpha_l \left.\frac{\partial \tilde{\rho}_l'}{\partial p}\right|_{\alpha_v}. \tag{49}$$

The term V_p is some characteristic velocity scale, typically the local convective velocity under inviscid conditions. The above formulation is, in fact, the same as that used by Kunz *et al*. for incompressible two-phase mixtures [11]. An interesting aspect of the above definition is that it is not possible to automatically switch the preconditioning off for supersonic flows as is typically done for single-phase flows [16–18]. While this is a disadvantage, the effect appears to be small in practice for moderate supersonic Mach numbers.

An alternate scaling choice is that corresponding to Eqs. (39) and (40). Accordingly,

$$\left.\frac{\partial \tilde{\rho}_v'}{\partial p}\right|_{\alpha_v} = \frac{1}{M^2}\left.\frac{\partial \tilde{\rho}_v}{\partial p}\right|_{\alpha_v}, \qquad \left.\frac{\partial \tilde{\rho}_l'}{\partial p}\right|_{\alpha_v} = \frac{1}{M^2}\left.\frac{\partial \tilde{\rho}_l}{\partial p}\right|_{\alpha_v}, \tag{50}$$

where $M^2 = V_p^2/c^2$, and V_p is some characteristic velocity scale. The above formulation is, in fact, identical to that proposed by Ahuja *et al*. [13] for isothermal multiphase mixtures. Further, it has the advantage of enabling the preconditioning to be turned off at supersonic speeds ($M \geq 1$), at which limit the equations are naturally well posed and well conditioned. However, implementation of the method in the incompressible limit is a little clumsy because the Mach number tends to zero in this limit. In practice, this is not a major issue since the incompressible sound speed may be set to an arbitrarily large number. In this work, unless otherwise specified, we employ Eq. (50) to define the pseudo-properties in the preconditioning matrix.

In order to verify that eigenvalues of the preconditioned system are well behaved, we examine the system Jacobian,

$$\Gamma_\alpha^{p-1} A_\alpha = \begin{bmatrix} u\frac{(c')^2}{c^2} & 0 & \rho(c')^2 \\ X & u & Y \\ \frac{1}{\rho} & 0 & u \end{bmatrix}, \tag{51}$$

where

$$\frac{1}{(c')^2} = \rho\left(\frac{\alpha_l}{\tilde{\rho}_l}\left.\frac{\partial \tilde{\rho}_l'}{\partial p}\right|_{\alpha_v} + \frac{\alpha_v}{\tilde{\rho}_v}\left.\frac{\partial \tilde{\rho}_v'}{\partial p}\right|_{\alpha_v}\right) = \frac{1}{V_p^2} \tag{52}$$

$$X = \rho u (c')^2 \frac{\alpha_l \alpha_v}{\tilde{\rho}_l \tilde{\rho}_v} \left(\frac{\partial \tilde{\rho}_v}{\partial p}\bigg|_{\alpha_v} \frac{\partial \tilde{\rho}'_l}{\partial p}\bigg|_{\alpha_v} - \frac{\partial \tilde{\rho}_l}{\partial p}\bigg|_{\alpha_v} \frac{\partial \tilde{\rho}'_v}{\partial p}\bigg|_{\alpha_v} \right) \tag{53}$$

$$Y = \rho (c')^2 \alpha_l \alpha_v \left(\frac{1}{\tilde{\rho}_l} \frac{\partial \tilde{\rho}'_l}{\partial p}\bigg|_{\alpha_v} - \frac{1}{\tilde{\rho}_v} \frac{\partial \tilde{\rho}'_v}{\partial p}\bigg|_{\alpha_v} \right). \tag{54}$$

The eigenvalues of the preconditioned two-phase system are given as

$$u, \frac{1}{2}\left[u\left(1 + \frac{(c')^2}{c^2}\right) \pm \sqrt{u^2\left(1 - \frac{(c')^2}{c^2}\right)^2 + 4(c')^2} \right]. \tag{55}$$

Since $(c')^2 = V_p^2$, the "acoustic" eigenvalues in the above expression are of the same order as the particle speed, thereby ensuring well-conditioned eigenvalues at all speeds. We note that the above expressions for the Jacobian and eigenvalues hold for both the Kunz *et al.* [11] scaling in Eq. (48) and the Ahuja *et al.* [13] scaling in Eq. (50). Finally, we also note that the above formulation reduces to Chorin's artificial compressibility for single-phase incompressible flows [15] and to standard preconditioning for single-phase compressible flows [16–18].

5.2. Mass Fraction Form

A slightly different formulation results if we start with the mass fraction form of the governing equations (Eq. (19)). We may now write the preconditioning system as

$$\Gamma_Y^p \frac{\partial Q_Y}{\partial \tau} + \frac{\partial E}{\partial x} = 0, \tag{56}$$

with the preconditioning matrix being defined as

$$\Gamma_Y^p = \begin{bmatrix} Y_v \frac{\partial \rho'}{\partial p}\big|_{Y_v} & \rho + Y_v \frac{\partial \rho}{\partial Y_v}\big|_p & 0 \\ Y_l \frac{\partial \rho'}{\partial p}\big|_{Y_v} & -\rho + Y_l \frac{\partial \rho}{\partial Y_v}\big|_p & 0 \\ u \frac{\partial \rho'}{\partial p}\big|_{Y_v} & u \frac{\partial \rho}{\partial Y_v}\big|_p & \rho \end{bmatrix}. \tag{57}$$

Using Eq. (45), we may write

$$\frac{\partial \rho'}{\partial p}\bigg|_{Y_v} = \frac{1}{c'^2} = \frac{1}{V_p^2}, \tag{58}$$

and V_p is again some reference velocity scale.

The above formulation is identical to the preconditioning used for reacting gas mixtures [18] and is also similar to that proposed by Merkle *et al.* for two-phase flows [10]. It reduces to Chorin's artificial compressibility for incompressible single-phase flows and to the standard preconditioning form for compressible single-phase flows. It can also be readily shown that the eigenvalues of the above formulation are the same as the eigenvalues of the preconditioned volume fraction formulation (Eq. (55)).

We further note that the preconditioned system in Eq. (56) may be transformed to the volume fraction variables through the application of a simple chain rule. However, the

resulting system remains different from the preconditioned volume fraction form given in Eq. (46). Thus, the two formulations are not identical, but they are closely related and possess the same eigenvalues. Our experience suggests that both approaches should perform equally well in practice and that the decision of which one to use may well depend upon the particular form of the equations and solution variables used in the candiate code. In the current paper, we have used the volume fraction form (Eq. (46)).

6. COMPUTATIONAL FORMULATION

The preconditioning system for isothermal compressible multiphase flows has been incorporated into the UNCLE-M code. This code was originally developed for incompressible flows at Mississippi State University [19]. Subsequently, it has been extensively revised and extended to two-phase mixtures by Kunz *et al.* [11]. The code is structured, multiblock, implicit, and parallel, with upwind flux-difference splitting for the spatial discretization with appropriate flux limiters and Gauss–Seidel relaxation for the inversion of the implicit operator. It must be emphasized that the flux difference formulation is based upon the preconditioned time-derivatives in order to ensure reliable accuracy under all conditions. Further details regarding the numerical method are identical to those given in Ref. [11] with the exception that, to form the numerical fluxes, we have applied the van Albada TVD limiter.

The time-marching formulation for the multiphase system with compressibility effects is as follows:

$$\Gamma_p^{\alpha} \frac{\partial Q_{\alpha}}{\partial \tau} + \frac{\partial Q}{\partial t} + \frac{\partial E_j}{\partial x_j} = H. \tag{59}$$

Note that a dual-time formulation has been adopted with the first time-derivative representing the pseudo-time-derivative (used for purposes of the time-iterative procedure), while the second time-derivative is the physical time-derivative (required for resolving unsteady flow phenomena) [18].

The physical time-derivative, flux vectors, and source terms are given as follows:

$$Q = \begin{bmatrix} \tilde{\rho}_v \alpha_v \\ \tilde{\rho}_l \alpha_l \\ \rho u_i \end{bmatrix}, \qquad E_j = \begin{bmatrix} \tilde{\rho}_v \alpha_v u_j \\ \tilde{\rho}_l \alpha_l u_j \\ \rho u_i u_j + p\delta_{ij} - \mu_{m,t}\sigma_{ij} \end{bmatrix}, \qquad H = \begin{bmatrix} -(\dot{m}^+ + \dot{m}^-) \\ (\dot{m}^+ + \dot{m}^-) \\ (0)_i \end{bmatrix}. \tag{60}$$

Note that the viscous fluxes have been included in the momentum equations, and source terms describing the transfer of mass between the liquid and vapor states are included in the phasic continuity equations. Turbulent eddy viscosity is determined using a standard wall-function-based $k - \varepsilon$ model. Further, for flows with a noncondensable gas, an additional gaseous transport equation is introduced.

The mass transfer terms are described using simple finite-rate relations:

$$\dot{m}^+ = \frac{C_{prod} \tilde{\rho}_v \alpha_l^2 (1 - \alpha_l)}{t_{\infty}} \tag{61}$$

$$\dot{m}^- = \frac{C_{dest} \tilde{\rho}_v \alpha_l \mathrm{MIN}[0,\, p - p_v]}{\frac{1}{2}\rho_{\infty} U_{\infty}^2 t_{\infty}}. \tag{62}$$

Here, thermal effects on the phase change have been neglected. C_{prod} and C_{dest} are empirical constants, and t_∞ is a mean flow timescale. For the results presented here, $C_{prod} = 1$, $C_{dest} = 10^5$, and $t_\infty = 1$. We point out that the mass transfer terms are phenomenological models and the choice of constants is somewhat arbitrary. However, our experience, as well as that of other researchers, suggests that the results are relatively insensitive to the precise values used [10–14].

The pseudo-time-derivatives are responsible for driving to convergence the unsteady equations at each physical time level. Accordingly, the pseudo-time-derivatives are preconditioned for optimal performance as discussed in the previous sections. The multidimensional forms of these terms are

$$Q_\alpha = \begin{bmatrix} p \\ \alpha_v \\ u_i \end{bmatrix} \qquad \Gamma^p_\alpha = \begin{bmatrix} \alpha_v \frac{\partial \tilde{\rho}'_v}{\partial p}\Big|_{\alpha_v} & \tilde{\rho}_v & 0 \\ \alpha_l \frac{\partial \tilde{\rho}'_l}{\partial p}\Big|_{\alpha_v} & -\tilde{\rho}_l & 0 \\ u_i \frac{\partial \rho'}{\partial p}\Big|_{\alpha_v} & u_i(\tilde{\rho}_v - \tilde{\rho}_l) & \rho\delta_{ij} \end{bmatrix}, \tag{63}$$

with the primed property variables being defined as in Eq. (50).

The characteristic velocity parameter in these definitions is generally expressed as some functional combination of the free-stream and the local convective velocity scales,

$$V_p^2 = \mathrm{Min}\big(\mathrm{Max}\big(V^2, kV_\infty^2\big), c^2\big), \tag{64}$$

where V is the local convective velocity and V_∞ is the free-stream velocity. This definition is similar in form to that suggested by Turkel [16]. We note that the factor k is typically provided as a user-specified parameter and is somewhat dependent upon the frequency of the unsteady processes being analyzed [18]. More refined definitions of the reference velocity based upon local unsteady phenomena will be the subject of future study.

Further numerical details on the physical time-stepping, the pseudo-time-stepping, the spatial discretization, and the implicit solution procedure are given in Ref. [11].

7. RESULTS

The main purpose of this paper is the formulation of a time-marching procedure for the solution of multiphase homogenous mixture flows including compressibility effects. Here, we present some demonstrative results for multiphase problems, many of which involve transonic and supersonic flows. We begin with a simple one-dimensional shock tube problem, for which an exact analytical solution exists. We then consider natural cavitation on submerged bodies, a case that we have previously studied using a fully incompressible multiphase model [11, 12]. Here, we assess the influence of including compressibility effects on this flowfield. Finally, we consider two applications that involve supersonic multiphase flows, namely, a supersonic underwater projectile and a supersonic underwater rocket plume. The results showcase the capabilities of the formulation to handle a rich variety of multiphase problems involving compressibility effects.

7.1. Shock-Tube Problem

As a first example, we consider the unsteady two-phase shock-tube problem investigated both experimentally and theoretically by Campbell and Pitscher [5]. The problem can be

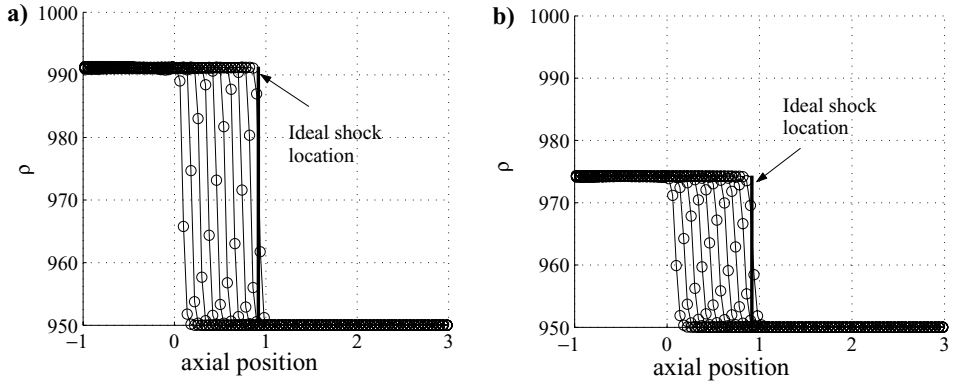

FIG. 2. Mixture shock-tube computations and comparison with theory of Campbell and Pitscher [5]. Shock moves from left to right with initial location at 0. Model solution shown at even time intervals beginning after initial state. Fluid to right of shock is at rest with liquid-to-gas density ratio of 1000, and $\alpha_l = 0.95$. (a) Pressure ratio 2. (b) Pressure ratio 6.

modeled as a shock wave moving into a stationary and noncondensable, nonvaporizable gas/liquid mixture. Assuming that the liquid is incompressible and the gas is perfect, an exact expression may be obtained for the shock speed [5],

$$u_1^2 = \frac{p_2}{p_1} c_1^2, \tag{65}$$

where the subscript 1 denotes conditions in front of the shock, the subscript 2 denotes conditions behind it, and u_1 is the shock speed.

Figure 2 shows the results for two different pressure ratios of 2 and 6. The calculations are carried out using 101 axial grid points and are second-order accurate in time and third-order accurate in space. The flow is initially at rest with the shock initially at the zero axial position. In each case, the predicted results after a given period of time are compared with the theoretical shock location, and very good agreement is obtained. We note here that the time-accurate results were obtained using dual time-stepping. The characteristic velocity parameter, V_p, is specified to be the speed of sound, which is representative of the characteristic timescale associated with the shock motion. The results demonstrate that the two-phase preconditioning formulation is capable of resolving acoustic/compressibility effects very well.

7.2. Natural Cavitation on Axisymmetric Bodies

The application of principal interest to us involves the modeling of sheet cavitation around axisymmetric bodies at high Reynolds numbers. Because of their importance to naval hydrodynamics applications, numerous experimental and computational studies of cavity flowfields around bodies of different shapes have been carried out. Rouse and McNown have documented steady and time-averaged measurements of relevant cavitation parameters for various forebody shapes [20]. May has assembled cavity shape and size parameters for a wide range of cavitation numbers [21]. Stinebring *et al*. have documented the unsteady cycling behavior of several axisymmetric cavitators [22]. Recently, Kunz *et al*. and Lindau *et al*. have modeled sheet cavity flowfields in a variety of configurations using an

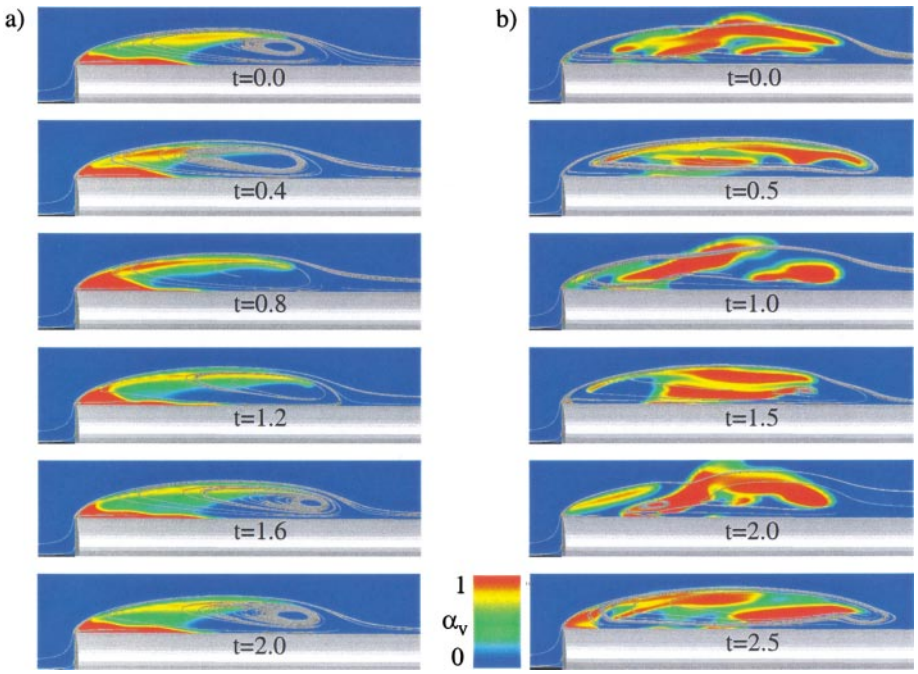

FIG. 3. Volume fraction contours and streamlines. Snapshots span an approximate modeled cycle. 0-caliber ogive at $\mathrm{Re_D} = 1.46 \times 10^5$ and $\sigma = 0.3$. (a) Isothermal compressible form. (b) Incompressible form. Blue is liquid ($\alpha_v = 0$) and red is vapor ($\alpha_v = 1$). Time is given in model units referred to the initialization of the cycle, $D/U_\infty = 0.146$ model time units.

incompressible mixture model [11, 12]. They have made extensive comparisons with experimental data and have determined the strengths and shortcomings of their model. In this section, we perform similar computations with the current isothermal compressible model.

Figures 3 and 4 show flowfield snapshots of the unsteady cavitating flow over a 0-caliber ogive (20,288 grid points in the plane displayed) and a 1/4-caliber ogive (16,705 grid points in the plane displayed). The calculations are axisymmetric and have been carried out using three-dimensional grids with a single computational cell in the direction of symmetry. Each domain is comprised of multiple structured grid blocks. The computations are second-order accurate in time and space. The Reynolds numbers are approximately 1.4×10^5 and the cavitation number is 0.3. In both sets of figures, corresponding results using the incompressible mixture model have also been included to facilitate direct comparison.

It is evident that the flowfields are rich in complexity. We first consider the 0-caliber results in Fig. 3. Both incompressible and compressible results show the cavity forming at or very near the leading edge of the ogive body. The cavity is observed to be composed almost entirely of low-density vapor. Further, because of the sharp turning of the incoming flow, a recirculating bubble is also formed in this cavity region. The incoming liquid then flows over the bubble and rejoins the surface of the body downstream of the cavity and the recirculating bubble. The pressure recovery in this downstream region then sets up a liquid reentrant jet which shoots into the cavity. As we follow the snapshots through a complete period, we observe that this reentrant jet appears to progress deeper into the cavity until some form of cavity pinching occurs that causes the jet to retract until the cycle can commence

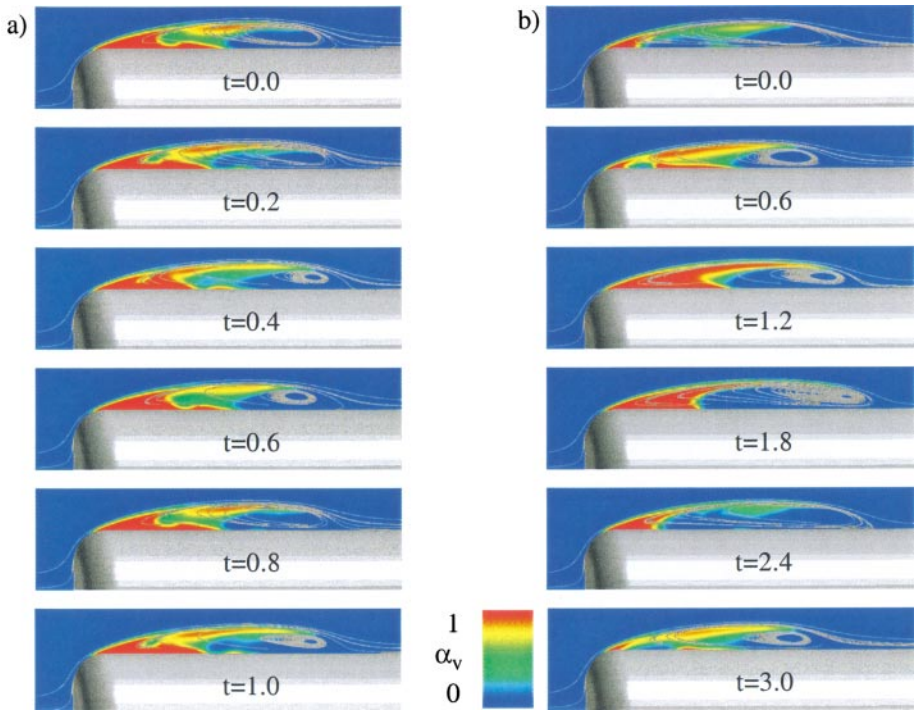

FIG. 4. Volume fraction contours and streamlines. Snapshots span an approximate modeled cycle. 0.25-caliber ogive at $\mathrm{Re_D} = 1.36 \times 10^5$ and $\sigma = 0.3$. (a) Isothermal compressible form. (b) Incompressible form. Blue is liquid ($\alpha_v = 0$) and red is vapor ($\alpha_v = 1$). Time is given in model units referred to the initialization of the cycle, $D/U_\infty = 0.136$ model time units.

again. The unsteady cycle thus seems to be closely coordinated with the reentrant jet and the cavity pinching process.

Figure 3 shows a marked difference between the compressible and incompressible results in the extent to which the liquid reentrant jet penetrates the cavity. In the compressible case, the liquid jet traverses only about one-half of the cavity length before the jet is pinched off and begins to retract. The incompressible case also shows the reentrant jet getting pinched off; however, the liquid bubble appears to remain intact within the cavity until it reaches the leading edge. In fact, at $t = 0.5$, the reentrant liquid appears to have pushed the cavity downstream of the leading edge.

This difference between the compressible and incompressible results is also observed in Fig. 4 for the 1/4-caliber case. In fact, the difference appears even more marked, with the compressible case showing the liquid reentrant jet barely reaching into one-half the length of the cavity, while in the incompressible result, it again appears to traverse most of the cavity length.

These trends in the behavior of the reentrant jet appear to control the unsteady dynamics of the flowfields. Figures 5 and 6 show the instantaneous (pressure) drag coefficient histories for the two cases. The drag coefficient is essentially a measure of the total pressure on the face of the ogive body. The fluctuations in this quantity then result from the upstream propagation of pressure disturbances generated by the cavity pulsations.

Examination of the 0-caliber drag coefficient histories in Fig. 5 reveals that the incompressible amplitudes are significantly higher, a fact that is reflected by the more extreme

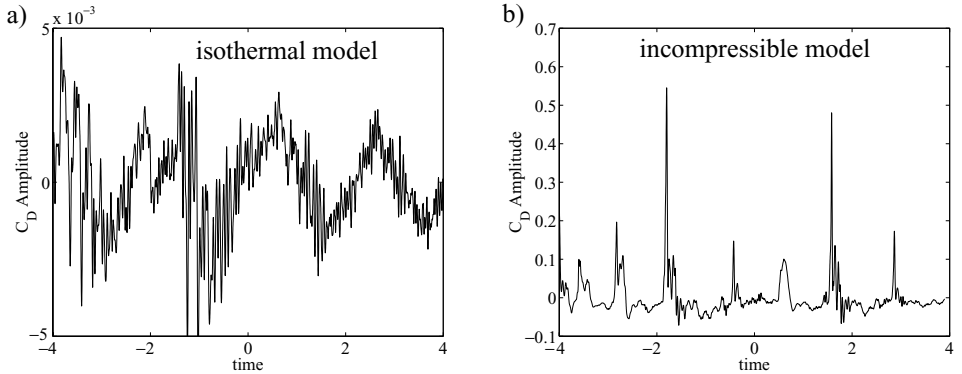

FIG. 5. Drag coefficient histories for 0-caliber ogive shape modeled with isothermal compressible and incompressible forms. Time is given in model units referred to the initialization of the cycle, $D/U_\infty = 0.146$ model time units.

cavity distortions that are evident in the incompressible snapshots in Fig. 3. Further, the dominant mode of the compressible result shows a slightly higher frequency than the incompressible result. Again, this result appears to correlate with the distance traversed by the reentrant jet in Fig. 3, with the shorter reentrant jet penetration yielding the higher frequency.

Drag coefficient results for the 1/4-caliber ogive are given in Fig. 6. Here, both incompressible and compressible amplitudes are observed to be small, in accordance with the more streamlined cavity shapes evident in the snapshots in Fig. 4. However, there is now a more significant difference in the cycling frequency, with the compressible case showing a much higher frequency. Again, this result correlates well with the jet penetration distance in Fig. 4. The incompressible case shows the reentrant jet reaching much deeper into the cavity and, hence, has a smaller cycling frequency.

The frequency data for the above cases are compared with measurement data obtained by Stinebring *et al.* [22] in Fig. 7. While all the computed data lie within the bounds of the

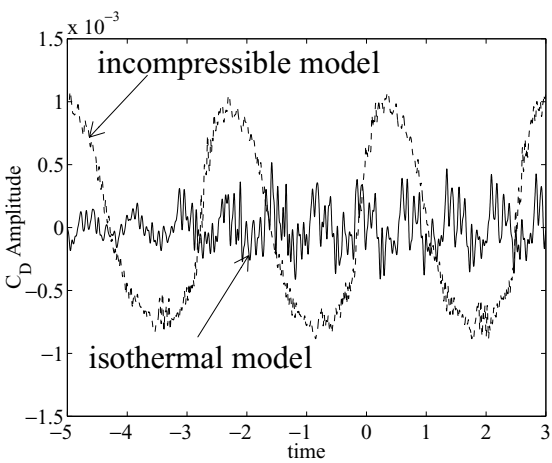

FIG. 6. Drag coefficient histories for 1/4-caliber ogive shapes modeled with incompressible and isothermal compressible forms. Time is given in model units referred to the initialization of the cycle, $D/U_\infty = 0.146$ model time units.

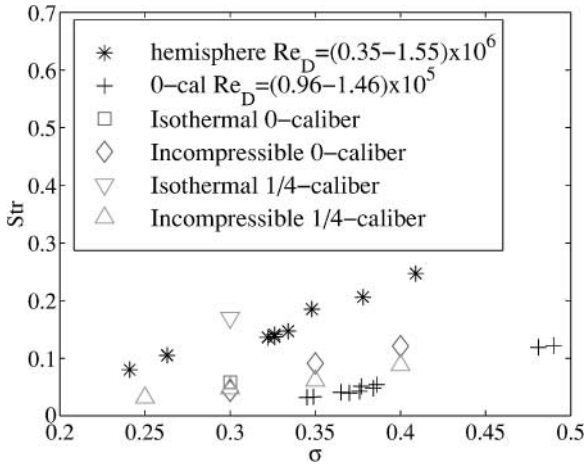

FIG. 7. Strouhal frequency $(fD)/(U_\infty)$ comparison modeling results and data from Stinebring *et al.* [22].

experimental data, it is interesting that the experimental data for the hemispherical forebody indicate a higher Strouhal frequency than the corresponding result for the 0-caliber ogive. We point out that this trend is in agreement with the higher frequency obtained for the 1/4-caliber ogive using the compressible model. On the other hand, the incompressible model predicts roughly the same Strouhal frequency for the two shapes.

The above comparison suggests that the compressible model may be capturing the dynamics of the cavity more correctly than the incompressible model. In particular, it appears that the penetration of the liquid jet (in Fig. 4) may be overpredicted by the incompressible model. It is not immediately apparent why this may be the case. We speculate that the compressible nature of the vapor phase may be causing the pressure within the cavity to increase somewhat during the jetting process, thereby weakening the penetration of the jet. In the incompressible case, on the other hand, the vapor phase is treated as an incompressible fluid, which may readily accommodate the incoming jet by expanding the size of the cavity as a whole. Of course, these observations are preliminary in nature and detailed computations over a range of cavitation numbers are necessary to reach definitive conclusions.

Extensive time-averaged data are also available to characterize various cavity parameters. Figure 8 shows a comparison of arithmetically averaged data for the 0-caliber and

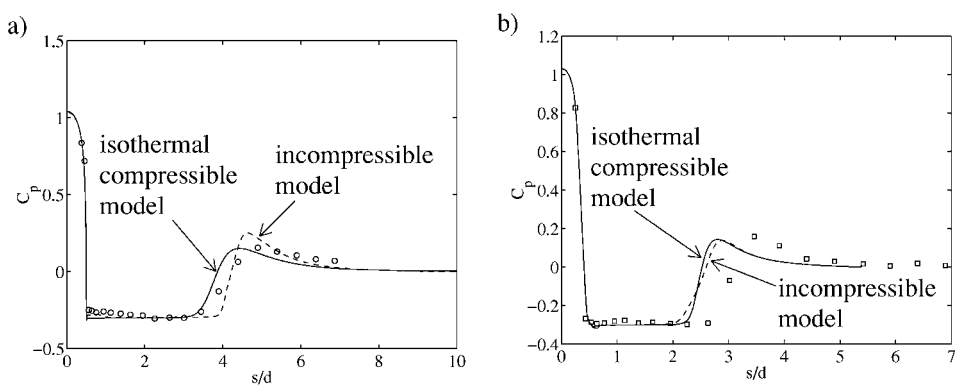

FIG. 8. Comparison of time-averaged results with data of Rouse and McNown [20]. (a) 0-caliber. (b) 1/4-caliber.

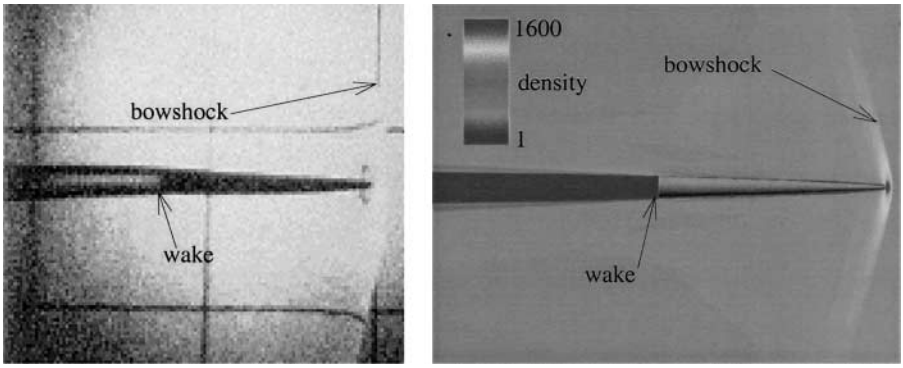

FIG. 9. Photograph [23] and isothermal compressible model result of supersonic underwater projectile. Model result contains flowfield density contours indicating bowshock and vaporous wake.

1/4-caliber ogive cases with average surface pressure measurements from Rouse and McNown [20]. The incompressible results are also included for comparison. In all cases, the computed data generally agree with the experiments. Although there are some differences between the compressible and incompressible results, both sets appear to compare well with the data.

7.3. Other Applications

In this section, we briefly consider two other applications of interest that involve the modeling of two-phase compressibility effects. Figure 9 shows an underwater supersonic projectile. Both computational results and a corresponding photograph [23] of an actual test are included in the figure. The three-dimensional, but axisymmetric, computational grid is comprised of 48,049 (in the plane displayed) grid points, and second-order spatial accuracy is used. The flow Mach number for the case shown is 1.03 and the liquid-to-gas density ratio

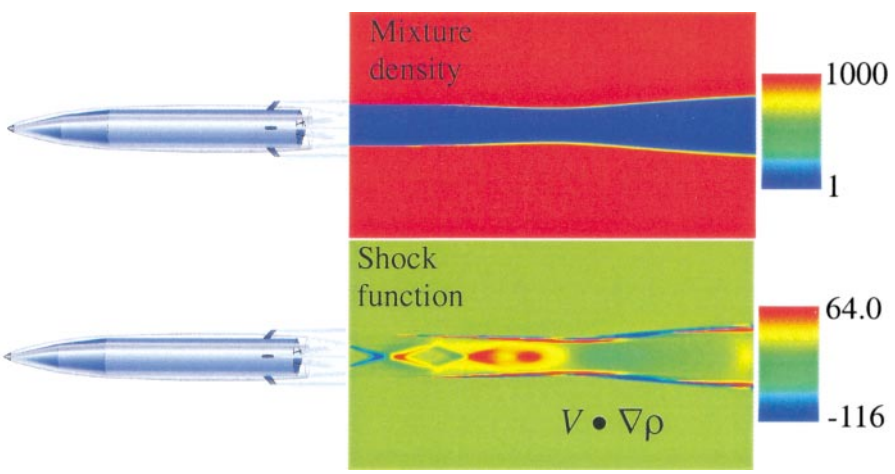

FIG. 10. Cartoon vehicle and three-stream, axisymmetric aft flow region. Supersonic gas center jet (diameter = 1), surrounded by subsonic gas (at free-stream velocity with outer diameter = 2), surrounded by subsonic liquid. Liquid-to-gas density ratio 1000.

is nominally 1000. The experiments and the computations show the presence of a bowshock upstream of the nose. In addition, because of the high velocity, the cavitation number is about 10^{-4}. Consequently, with the exception of the nose, which is in compression, the flow immediately adjacent to the body is completely vaporized, as is the downstream wake portion.

The second example, shown in Fig. 10, is the plume flowfield of an underwater rocket exhaust. The plume exhaust is supersonic and is slightly underexpanded. It is surrounded by a coflowing secondary subsonic gas stream, which in turn is surrounded by a liquid water freestream flow. The nominal liquid-to-gas density ratio is 1000. The two-dimensional computational grid is comprised of 33,153 grid points and second-order spatial accuracy is used. Figure 10 shows the shock function field, which exhibits the classic expansion pattern. In particular, the interaction of the compressible gas stream with the incompressible liquid is demonstrated first by the contraction and then by the expansion of the gas stream. In addition, the interface between the liquid and gas phases is comprised of a two-phase mixture, which is also fully supersonic due to the low magnitude of the mixture sound speed.

Both of the above examples involve supersonic Mach numbers in the bulk flow for at least one of the phases. The current isothermal assumption may be inadequate to fully represent the dynamics of these flowfields. Nevertheless, these preliminary results demonstrate the ability of the algorithm to handle compressibility effects. Detailed modeling of such flowfields using a fully compressible two-phase formulation (including the energy equation) will be the subject of future research.

8. SUMMARY

Multiphase mixture flows present a unique challenge to CFD algorithms because of the simultaneous presence of incompressible flow in the liquid phase, low-speed compressible flow in the vapor phase, and transonic and supersonic flows in the two-phase mixture region. Moreover, in certain applications, the bulk liquid flow may also be transonic or supersonic. Thus, multiphase CFD algorithms have to be efficient and accurate over a wide range of Mach number regimes and have to be capable of capturing compressible phenomena.

We have developed a preconditioned time-marching algorithm for the computation of multiphase mixture flows. The derivation is based upon carrying out perturbation expansions of the underlying time-dependent system and examining the forms of the equations in the asymptotic limit. The preconditioning formulation introduces pseudo-time-derivatives, which automatically adapt to keep the system well conditioned in the incompressible as well as the compressible regimes, and thereby ensures that proper accuracy and optimal efficiency are maintained at all flow conditions. Three closely related but distinct preconditioning formulations have been derived for the isothermal compressible multiphase system. The differences arise from the precise form of the governing equations, volume or mass fraction, used in the derivation. However, we have shown that all three systems possess identical eigenvalues and should, therefore, perform comparably in practice.

The volume fraction form of the preconditioning algorithm has been incorporated into an existing multiphase code (UNCLE-M) and applied to simple as well as practical application problems. Our principal interest is the modeling of sheet- and supercavitating flowfields in hydrodynamics applications. Computational results were obtained for flow over 0-caliber and 1/4-caliber ogives and compared with experimental data as well as with previously obtained incompressible results. The computed compressible and incompressible results

agree well with each other and with the experiments for time-averaged data. The unsteady results, however, show some marked differences between the compressible and incompressible cases. The flowfields are characterized by unsteady effects caused by cavity reentrant liquid jets and cavity pinching. In the compressible case, the cavity reentrant jets appear to be relatively short-lived compared with the incompressible case. In the latter case, the reentrant jet persists almost until it reaches the leading edge of the cavity. In turn, these effects lead to higher frequencies for the compressible model, which is in agreement with measured Strouhal frequency data. Thus, it appears that compressibility effects may need to be considered to correctly describe the cavity dynamics. Additional investigations over a wider range of cavitation numbers are necessary to confirm these findings.

Preliminary computations have also been performed for underwater supersonic projectile and underwater rocket plume flowfields. Results with the present isothermal compressible formulation appear to be qualitatively correct. However, because the bulk flow of one of the phases is supersonic, a fully compressible formulation (including the energy equation) may be necessary to accurately model the flowfields. The development of algorithms for the fully compressible multiphase system is currently underway. In addition, future work will include detailed assessments of viscous, unsteady, and source term effects on the behavior of multiphase algorithms.

ACKNOWLEDGMENTS

This work is supported by the Office of Naval Research, Grants N00014-98-1-0143 and N00014-01-1-0325, with Dr. Kam Ng as contract monitor.

REFERENCES

1. R. Eddington, Investigation of supersonic phenomena in a two-phase (liquid gas) tunnel, *AIAA J.* **8**(1), 65 (1970).
2. J. Witte, Mixture shocks in two-phase flow, *J. Fluid Mech.* **36**(4), 639 (1969).
3. L. Van Wijngaarden, One-dimensional flow of liquids containing small gas bubbles, *Annu. Rev. Fluid Mech.* **4**, 369 (1972).
4. G. E. Reisman, Y. C. Wang, and C. E. Brennen, Observations of shock waves in cloud cavitation, *J. Fluid Mech.* **355**, 255 (1998).
5. I. J. Campbell and A. S. Pitscher, Shock waves in a liquid containing gas bubbles, *Proc. R. Soc.* **A234**, 534 (1958).
6. I. Toumi, A. Kumbaro, and H. Paillere, *Approximate Riemann Solvers and Flux Vector Splitting Schemes for Two-Phase Flow, VKI Lecture Series 1999-03* (von Karman Institute for Fluid Dynamics, Rhode Saint Genese, Belgium, 1999).
7. P. Wesseling, *Non-Convex Hyperbolic Systems, VKI Lecture Series 1999-03* (von Karman Institute for Fluid Dynamics, Rhode Saint Genese, Belgium, 1999).
8. M.-S. Liou and J. R. Edwards, *AUSM Schemes and Extensions for Low Mach and Multiphase Flows, VKI Lecture Series 1999-03* (von Karman Institute for Fluid Dynamics, Rhode Saint Genese, Belgium, 1999).
9. C. S. Song and X. Chen, Numerical simulation of cavitating flows by single-phase flow approach, in *Proceedings of the 3rd International Symposium on Cavitation, Grenoble, France* (J. M. Michel and H. Kato, Eds., 1998).
10. C. L. Merkle, J. Z. Feng, and P. E. O. Buelow, Computational modeling of the dynamics of sheet cavitation, in *Proceedings of the 3rd International Symposium on Cavitation, Grenoble, France* (J. M. Michel and H. Kato, Eds., 1998).

11. R. F. Kunz, D. A. Boger, D. R. Stinebring, T. S. Chyczewski, J. W. Lindau, H. J. Gibeling, S. Venkateswaran, and T. R. Govindan, A preconditioned Navier–Stokes method for two-phase flows with application to cavitation prediction, *Comput. Fluids* **29**, 849 (2000).
12. J. W. Lindau, R. F. Kunz, D. A. Boger, D. R. Stinebring, and H. J. Gibeling, High Reynolds Number, unsteady multi-phase CFD modeling of sheet cavitation, *J. Fluid Eng.-T ASME* **124**(3), (2002).
13. V. Ahuja, A. Hosangadi, and S. Arunajatesan, Simulations of cavitating flows using hybrid unstructured meshes, *J. Fluid Eng.-T ASME* **123**(2), 331 (2001).
14. I. Senocak and W. Shyy, *A Pressure-Based Method for Turbulent Cavitating Flow Computations*, AIAA Paper 2001-2907 (2001).
15. A. J. Chorin, A numerical method for solving incompressible viscous flow problems, *J. Comput. Phys.* **2**, 12 (1967).
16. E. Turkel, Preconditioning techniques in computational fluid dynamics, *Annu. Rev. Fluid Mech.* **31**, 385 (1999).
17. Y.-H. Choi and C. L. Merkle, The application of preconditioning to viscous flows, *J. Comput. Phys.* **105**, 207 (1993).
18. S. Venkateswaran and C. L. Merkle, *Analysis of Preconditioning Methods for the Euler and Navier Stokes Equations, VKI Lecture Series 1999-03* (von Karman Institute for Fluid Dynamics, Rhode Saint Genese, Belgium, 1999).
19. L. K. Taylor, A. Arabshahi, and D. L. Whitfield, *Unsteady Three-Dimensional Incompressible Navier–Stokes Computations for a Prolate Spheroid Undergoing Time-Dependent Maneuvers*, AIAA Paper 95-0313 (1995).
20. H. Rouse and J. S. McNown, *Cavitation and Pressure Distribution, Head Forms at Zero Angle of Yaw*, Studies in Eng. *Bull.* **32** (State University of Iowa, 1948).
21. A. May, *Water Entry and the Cavity-Running Behavior of Missiles*, Naval Sea Systems Command Hydroballistics Advisory Committee Technical Report 75-2 (1975).
22. D. R. Stinebring, M. L. Billet, and J. W. Holl, *An Investigation of Cavity Cycling for Ventilated and Natural Cavities*, TM 83-13 (Pennsylvania State Univ. Press, University Park, PA, 1983).
23. I. N. Kirschner, Results of selected experiments involving supercavitating flows, in *RTO AVT/VKI Special Course on Supercavitating Flows* (von Karman Institute for Fluid Dynamics, Rhode Saint Genese, Belgium, 2001).